

**Behaviour of steel-reinforced concrete columns under combined torsion based on ABAQUS FEA**

Cao, Xiaoluo; Wu, Linmei; Li, Zhenming

**DOI**

[10.1016/j.engstruct.2019.109980](https://doi.org/10.1016/j.engstruct.2019.109980)

**Publication date**

2020

**Document Version**

Accepted author manuscript

**Published in**

Engineering Structures

**Citation (APA)**

Cao, X., Wu, L., & Li, Z. (2020). Behaviour of steel-reinforced concrete columns under combined torsion based on ABAQUS FEA. *Engineering Structures*, 209, Article 109980. <https://doi.org/10.1016/j.engstruct.2019.109980>

**Important note**

To cite this publication, please use the final published version (if applicable). Please check the document version above.

**Copyright**

Other than for strictly personal use, it is not permitted to download, forward or distribute the text or part of it, without the consent of the author(s) and/or copyright holder(s), unless the work is under an open content license such as Creative Commons.

**Takedown policy**

Please contact us and provide details if you believe this document breaches copyrights. We will remove access to the work immediately and investigate your claim.

# Behaviour of steel-reinforced concrete columns under combined torsion based on ABAQUS FEA

Xiaoluo Cao<sup>a,1</sup>, Linmei Wu<sup>b,c,1,\*</sup> [Linmei.Wu@usq.edu.au](mailto:Linmei.Wu@usq.edu.au), Zhenming Li<sup>d</sup>

<sup>a</sup>Department of Architecture and Civil Engineering, Shazhou Professional Institute of Technology, Zhangjiagang, China

<sup>b</sup>College of Civil Engineering, Suzhou University of Science and Technology, Suzhou 215011, China

<sup>c</sup>Centre for Future Materials, The University of Southern Queensland, Toowoomba, QLD 4350, Australia

<sup>d</sup>Department of Materials and Environment (Microlab), Faculty of Civil Engineering and Geoscience, Delft University of Technology, Delft, the Netherlands

\*Corresponding author at: Centre for Future Materials, The University of Southern Queensland, Toowoomba, QLD 4350, Australia.

<sup>1</sup>Supporting information: These authors contributed to the work equally and should be regarded as co-first authors.

---

## Abstract

A computational model for studying the mechanical performance of steel-concrete columns under combined torsion is established via ABAQUS. The model is validated by experimental results. Through numerical simulations, the influence of the axial load ratio, torsion-bending ratio, concrete strength, steel ratio, longitudinal reinforcement ratio, stirrup ratio, and shear-span ratio on the torsional behaviour of steel-concrete columns is comprehensively investigated. The initial torsion stiffness and ultimate torsion strength of the column increase with increasing concrete strength and decreasing shear-span ratio. The parameters in descending order of influence on the ultimate torsion strength are steel ratio, torsion-bending ratio, stirrup ratio, longitudinal reinforcement ratio, and axial load ratio. Furthermore, the seven parameters in descending order of influence on the ductility coefficient are the steel ratio, shear-span ratio, concrete strength, axial load ratio, stirrup ratio, torsion-bending ratio and longitudinal reinforcement ratio.

---

**Keywords:** ~~Steel-concrete column~~ steel-concrete composite column; Combined torsion; Numerical analysis; Torsion stiffness; Torsion strength; Ductility coefficient

# 1 Introduction

With the development of high-rise and large-span buildings, steel-reinforced concrete (SRC) structures with good overall seismic behaviour are widely used in engineering [1,2]. Meanwhile, with the increasing diversity of architectural styles and functional requirements, many complex and irregular structures have emerged. Corner columns in frame structures, particularly irregular structures, subjected to earthquakes are typically exposed to combined compression, bending, shear, and torsion. Due to the incorporation of torsion stress, the load-carrying capacity of a structural member can be lower than when subjected to a conventional combination of compression, bending, and shear load [3–5]. However, neither the two current Chinese design specifications [6,7] nor American and European standards provide design methods or calculation formulas for SRC members subjected to torsion. Relevant information on calculating the torsional capacity of SRC members by the superposition method are given only in Japanese specifications [8].

In references [9,10], the ANSYS finite element analysis (FEA) software was used to perform nonlinear analysis of SRC members subjected to torsion. The results showed that the stress of steel rebar (stirrups) was small when the concrete cracked; when the ultimate load was reached, part of the steel rebar (stirrups) could reach the yield strength, but the structural steel did not yield over the whole cross section. In reference [11], the ANSYS FEA software was used to carry out torsional analysis of SRC members. The results showed that the presence of torque affected the bending capacity of the members, and the torque and bending moment were correlated. A simplified method was proposed by [12] to calculate the cracking torque and the ultimate torque of an SRC member with H-shaped structural steel and a hollow SRC member with a rectangular steel tube under pure torsion. The experimental study on the pure torsion behaviour of SRC beams in references [13,14] showed that an optimized disposition of structural steel could greatly improve the torsional capacity and late-stage torsional stiffness of the members. Moreover, the ductility of the member could also be improved. In reference [15], 13 SRC beams were tested under pure torsion, and the failure characteristics, mechanism and crack development of SRC beams were obtained. The results of references [13,16] showed that the cracking torque and ultimate torque of SRC members subjected to compressive torsion increased with increasing axial compression ratio. However, the ductility of the composite decreased. In references [17–19], torsion tests of 23 rectangular and T-shaped SRC beams with different steel reinforcements were carried out. The results showed that increasing the volumetric steel ratio could effectively improve the ductility and torsional strength of SRC beams. Formulas for calculating the cracking torque and ultimate torque of angled SRC beams were then proposed by the authors. The behaviour of SRC columns under a combination of bending moment and torque was studied in [21]. The results showed that the bending strength of the members decreased by approximately 27% when a medium torque was applied, and a simplified equation for bending and torsion interaction was proposed. Kyungsik Kim [20] studied ultimate strengths of steel rectangular box beams subjected to combined action of bending and torsion, and the steel box beams were examined by a numerical approach using ABAQUS. Deifalla, A. [21] studied behaviour and analysis of inverted T-shaped RC beams under shear and torsion. Despite the abovementioned studies, the behaviour of SRC column specimens subjected to combined compression-bending-shear-torsion has not been well understood by either experiments or simulations.


Therefore, the aim of this study is to investigate the mechanical behaviour of SRC under combined compression-bending-shear-torsion. Considering the high costs and long times associated with experimental

studies, numerical simulation is a preferable method. Therefore, in the first part of this paper, a numerical simulation model is built. The model is then validated through experiments on six SRC columns under combined torsion load. In the third part of the paper, the effects of axial compression ratio, torsion-bending ratio, concrete strength, steel ratio, longitudinal reinforcement ratio, stirrup ratio and shear span ratio on the combined torsional behaviour of SRC columns are comprehensively studied through numerical simulation.

## 2 Experimental programme

For the experimental study, six half-scale H-shaped SRC columns were prepared, each with cross-sectional dimensions of  $b \times h = 300 \text{ mm} \times 300 \text{ mm}$  and a height of 900 mm. The distance between the horizontal loading point and the column base was  $H = 820 \text{ mm}$ . To simulate a fixed column base, a rectangular foundation with dimensions of  $120 \text{ mm} \times 500 \text{ mm} \times 460 \text{ mm}$  was attached to the column base. The column had a concrete cover thickness of 20 mm and a shear-span ratio of  $\lambda = M/Vh = H/h = 2.73$ . The structural steel was a hot-rolled H-shaped steel section made of Q235B steel, and the longitudinal and stirrup reinforcement was made of HRB400 rebar. The column longitudinal reinforcement was configured as  $8\Phi 12$ , with a longitudinal reinforcement ratio of 1%. Detailed design parameters and section details of the six specimens are shown in Table 1 and Fig. 1.

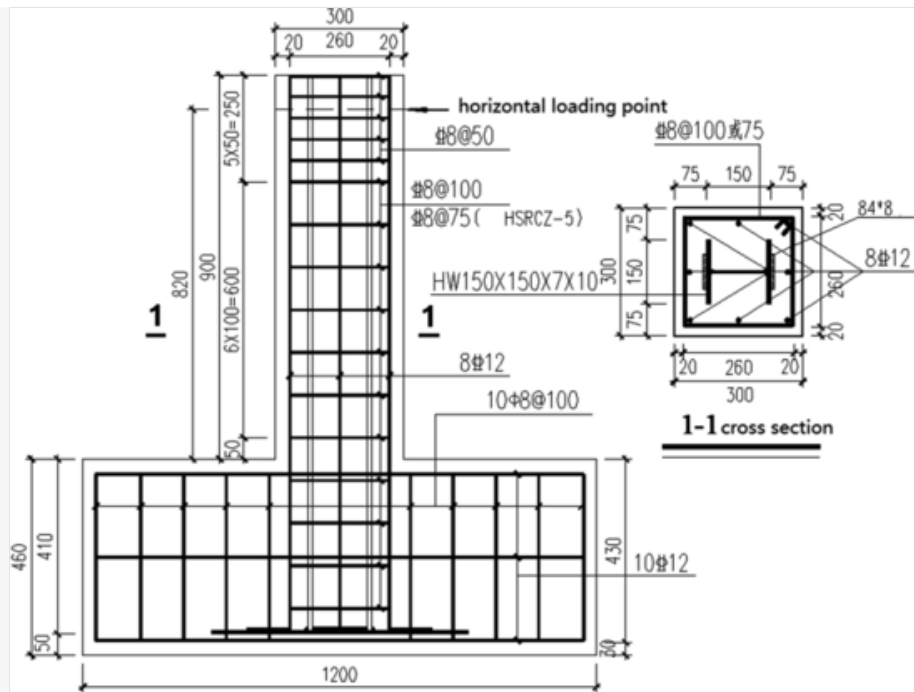
Table 1

 The presentation of Tables and the formatting of text in the online proof do not match the final output, though the data is the same. To preview the actual presentation, view the Proof.

Design parameters of the specimens.

Specimen no.	Axial load ratio	Torsion-bending ratio	Concrete strength $f_{cu}/\text{MPa}$	Steel ratio/%	Stirrup ratio/%
HSRCZ-1	0.1	1: 1	47.11	4.4	0.335
HSRCZ-2	0.2	1: 1	47.11	4.4	0.335
HSRCZ-3	0.2	1: 2	47.11	4.4	0.335
HSRCZ-4	0.1	1: 1	60.40	4.4	0.335
HSRCZ-5	0.1	1: 1	60.40	5.9	0.447
HSRCZ-6	0.1	1: 1	60.40	5.9	0.335

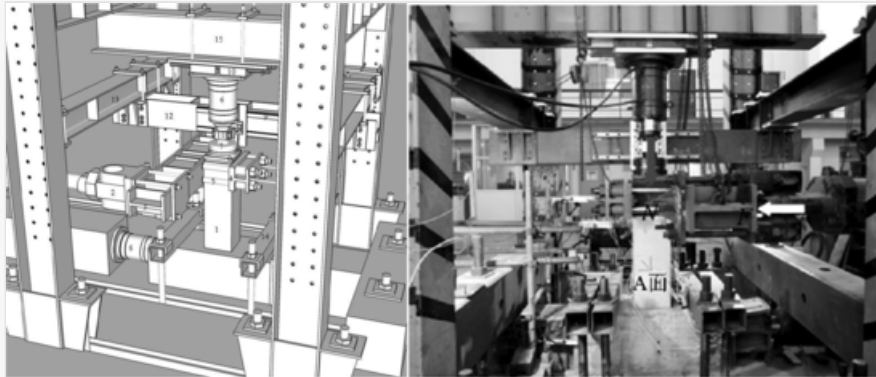
Fig. 1



Details of specimen design.

As shown in Fig. 2, the loading device was designed based on [22,6] and consisted of four systems: an eccentric horizontal loading system, a vertical loading system, a specimen top linear displacement guiding system, and a base displacement-limiting system, with the first three systems being the core of the loading device.

Fig. 2



Test loading device.

Monotonic loading was adopted in the experimental tests. First, a vertical force was applied to the specimen via a hydraulic jack until the predefined axial load was reached, and the load was then held constant. Next, a horizontal force was applied stepwise via an MTS servo actuator until the specimen failed.

### 3 Finite element model

### 3.1 Constitutive relationships of the materials

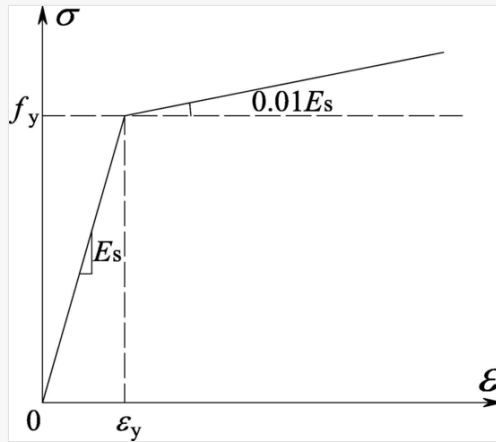
#### 3.1.1 Constitutive relationships of structural steel and reinforcement

The constitutive relationships of both structural steel and reinforcement in ABAQUS/CAE adopt a bilinear model with strain hardening. Large deformations of the materials were not considered. The actual stress and strain of the material were assumed to be identical to the nominal stress and strain, respectively. The stress-strain relationships of the structural steel and reinforcement are shown in Eq. (1) and Fig. 3.

$$\sigma_s = \begin{cases} E_s \varepsilon_s & 0 \leq \varepsilon_s \leq \varepsilon_y \\ f_y + 0.01E_s(\varepsilon_s - \varepsilon_y) & \varepsilon_s > \varepsilon_y \end{cases} \quad (1)$$

where  $\varepsilon_s$  is the steel strain,  $\sigma_s$  is the steel stress,  $\varepsilon_y$  is the steel yield strain,  $f_y$  is the steel yield stress, and  $E_s$  is the steel elastic modulus.

Fig. 3



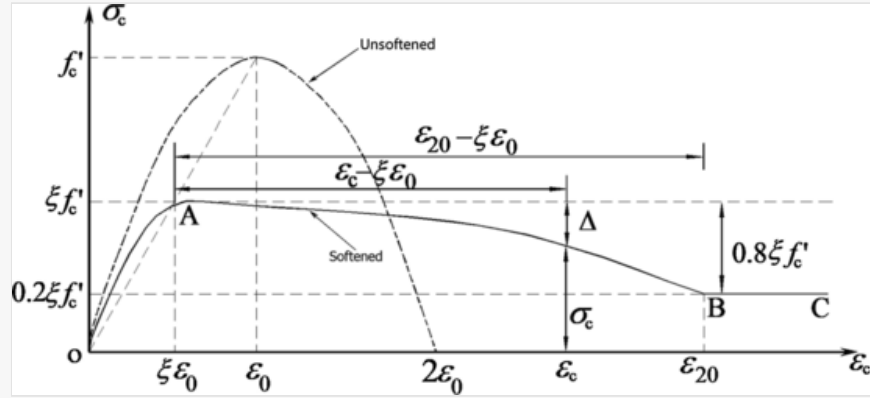
Constitutive relationships of the structural steel and reinforcement.

#### 3.1.2 Constitutive relationships of concrete

In view of the confining influence of the stirrup on the concrete, the softened membrane model (SMM) [23,24] and the Kent-Scott-Park model (KSPM) [25]—considering the concrete softening and the stirrup confinement, respectively—were used to model the different parts of the concrete within the column cross section separated by the outer edges of the stirrups.

The SMM mainly addresses the attenuation of the principal compressive stress of the concrete material under torsional shear stress—i.e., the so-called concrete softening phenomenon. This model introduces a softening coefficient  $\xi$  to modify the strain and stress of the peak in addition to the slope in the declining portion of the concrete compressive stress-strain relationship curve. The concrete compressive stress-strain relationship is shown in Eqs. (2)–(4) and Fig. 4.

Fig. 4

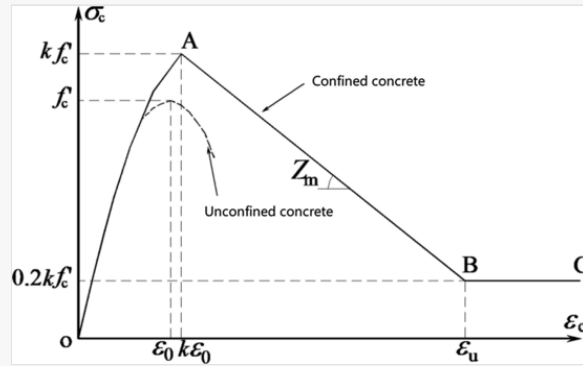


Compressive stress-strain relationship in the SMM.

OA portion (Fig. 5):

$$\sigma_c = \xi f'_c \left[ 2 \left( \frac{\epsilon_c}{\xi \epsilon_0} \right) - \left( \frac{\epsilon_c}{\xi \epsilon_0} \right)^2 \right] \quad 0 < \epsilon_c \leq \xi \epsilon_0 \quad (2)$$

Fig. 5



Compressive stress-strain relationship in the Kent-Scott-Park model.

AB portion:

$$\sigma_c = \xi f'_c \left[ 1 - \left( \frac{\epsilon_c / \xi \epsilon_0 - 1}{4 / \xi - 1} \right)^2 \right] \quad \xi \epsilon_0 < \epsilon_c \leq \epsilon_{20} \quad (3)$$

BC portion:

$$\sigma_c = 0.2\xi f'_c \quad \varepsilon_{20} < \varepsilon_c \quad (4)$$

where for concrete under C60,  $f'_c = 0.79f_{cu,k}$ ,  $\varepsilon_0 = 0.002$ , and  $\xi = \frac{5.8}{\sqrt{f'_c}} \frac{1}{\sqrt{1+400\varepsilon_1}} \left(1 - \frac{|\beta|}{24^\circ}\right)$ . In this expression,  $\varepsilon_1$  is the principal tensile strain in the vertical direction, and  $\beta$  is an eccentric angle calculated as  $\beta = \frac{1}{2} \tan^{-1} \left( \frac{\gamma_{21}}{\varepsilon_2 - \varepsilon_1} \right)$ .

The KSPM considers the confinement by the transverse stirrups by modifying the peak stress and peak strain in addition to the slope in the declining portion of the compressive stress-strain backbone curve of the concrete. The concrete compressive stress-strain relationship is shown in Eqs. (5)–(9) and Fig. 5:

OA portion:

$$\sigma_c = kf'_c \left[ 2 \left( \frac{\varepsilon_c}{k\varepsilon_0} \right) - \left( \frac{\varepsilon_c}{k\varepsilon_0} \right)^2 \right] \quad 0 < \varepsilon_c \leq k\varepsilon_0 \quad (5)$$

AB section:

$$\sigma_c = kf'_c \left[ 1 - Z_m(\varepsilon_c - k\varepsilon_0) \right] \quad k\varepsilon_0 < \varepsilon_c \leq \frac{0.8}{Z_m} + k\varepsilon_0 \quad (6)$$

BC portion:

$$\sigma_c = 0.2kf'_c \quad 0.8/Z_m + k\varepsilon_0 < \varepsilon_c \quad (7)$$

$$Z_m = \frac{0.5}{\frac{3+0.29f'_c}{145f'_c-1000} + 0.75\rho_{sv} \sqrt{\frac{h_c}{s_h}} - 0.002k} \quad (8)$$

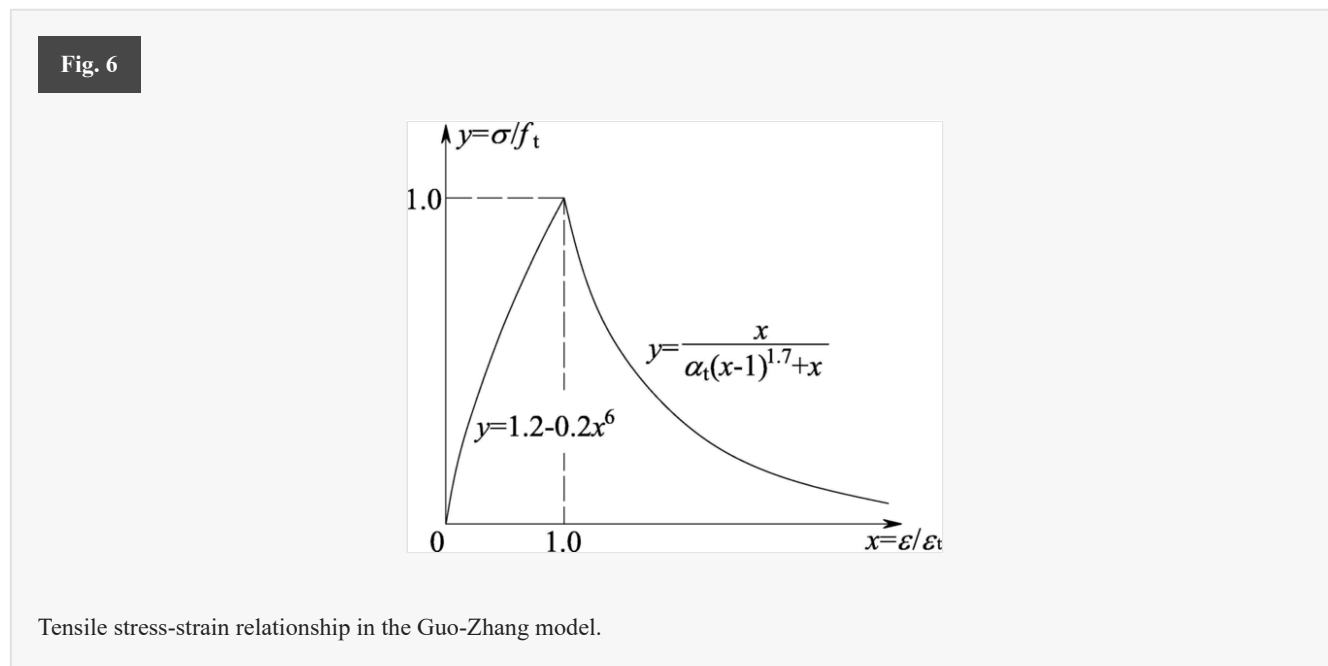
$$k = 1 + \rho_{sv} f_{yv} / f'_c \quad (9)$$

where  $k$  represents the confining increase coefficient of the stirrup for the concrete,  $\varepsilon_0$  is set to 0.002,  $Z_m$  is the slope of the strain-softening portion,  $f'_c = 0.67f_{cu,k}$ ,  $\rho_{sv}$  is the stirrup volume ratio of the column,  $h_c$  is the



width of the concrete enclosed by the outer edges of the confining stirrups,  $S_h$  is the stirrup spacing, and  $f_{yv}$  is the stirrup yield strength.

Many researchers have proposed many different concrete tensile constitutive models [23,26,27][26,27]. Qinghua university was adopted as the concrete tensile constitutive model. The stress-strain relation is shown in Eqs. (10)–(11) and Fig. 6.



When  $x \leq 1$ ,

$$y = 1.2x - 0.2x^6$$

(10)

When  $x > 1$ ,

$$y = \frac{x}{\alpha_t(x-1)^{1.7} + x}$$


(11)

where  $x = \varepsilon/\varepsilon_t$ ,  $y = \sigma/f_t$ , and  $\alpha_t = 0.312f_t^2$ , with  $f_t$  being the uniaxial tensile strength of concrete.

### 3.2 Element selection

The specimens mainly consisted of three parts: concrete, structural steel, and reinforcement cage. In the numerical simulation model, the dimensions of each part were consistent with those in the experiments. In addition, the slip between the structural steel, reinforcement, and concrete was considered. Instead, both the structural steel and reinforcement were “embedded” in the concrete. The selection of element types for various parts is listed in Table 2.

**Table 2**

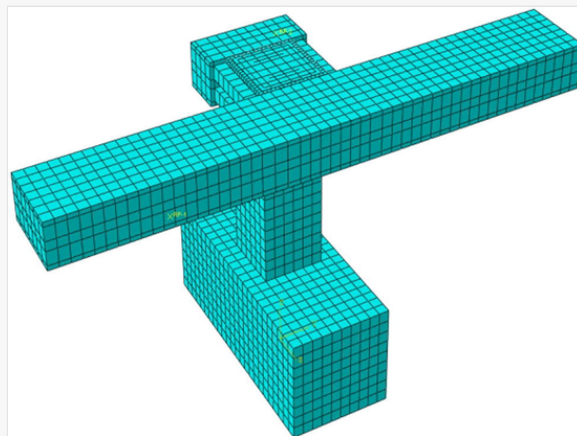
 The presentation of Tables and the formatting of text in the online proof do not match the final output, though the data is the same. To preview the actual presentation, view the Proof.

Material element selection.

Material	Concrete	Reinforcement	Structural steel
strength grade	C35/C45	HRB400	Q235B
selected element	C3D8R	T3D2	S4R

### 3.3 Construction of the numerical simulation model

If the loading device is omitted in the construction of the numerical simulation model, and a coupling reference point instead is established at the top of the column with a torsional angle and horizontal displacement simultaneously applied, then an issue arises regarding how to numerically determine the relative proportion between the horizontal bending displacement and torsional displacement. Therefore, based on the experimental results, a loading device was included in the numerical simulation model after necessary simplification. Specifically, the long and short loading beams were both simplified to cuboids with rectangular cross sections, and the tie rod was simplified to a cuboid with a square cross section. The final numerical simulation model is shown in [Fig. 7](#).

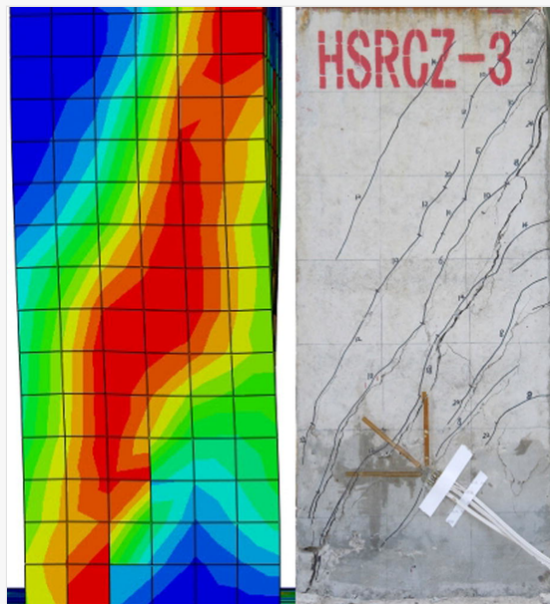
**Fig. 7**

Numerical simulation model.

## 4 Validation of the numerical simulation model

Monotonic static loading with displacement control was used in both the experimental tests and numerical simulation. Fig. 8 compares the tensile damage nephogram obtained from the numerical simulation with the surface cracks obtained from the experimental test of the same specimen HSRCZ-3.

Fig. 8

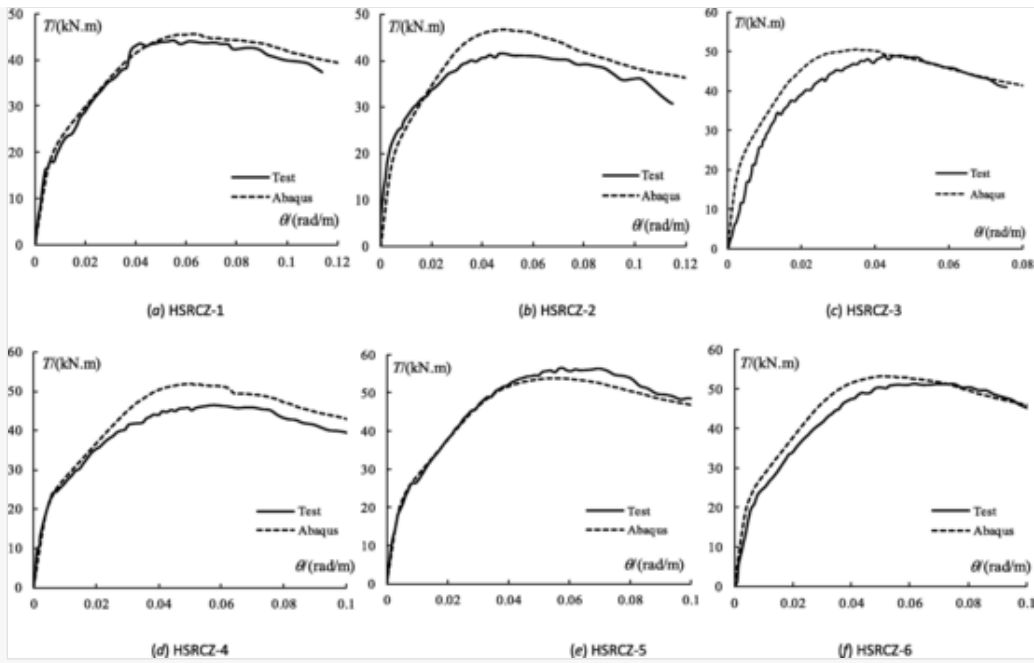


Comparison of the tensile damage nephogram and the test cracks.

Both the tests and numerical simulation show diagonal cracks in the  $60^\circ$  direction of the column. The peripheral box-shaped concrete subsequently cracks to form a variable-angle space truss, which resists the torque with the structural steel within the cross section.

Fig. 9 compares the numerical simulation results with the test results of the torque-twist curves of the six test specimens. It can be seen that in the elastic range prior to concrete crack formation, the test and numerical simulation torque-twist curves match well. In the elastoplastic range between the concrete cracking and the ultimate torque, the stiffness degradation of the test curve is generally slightly sharper than that of the numerical simulation curve (except for specimen HSRCZ-5). In the range of decreasing load-carrying capacity after the ultimate torque, the two curves demonstrate consistent trends.

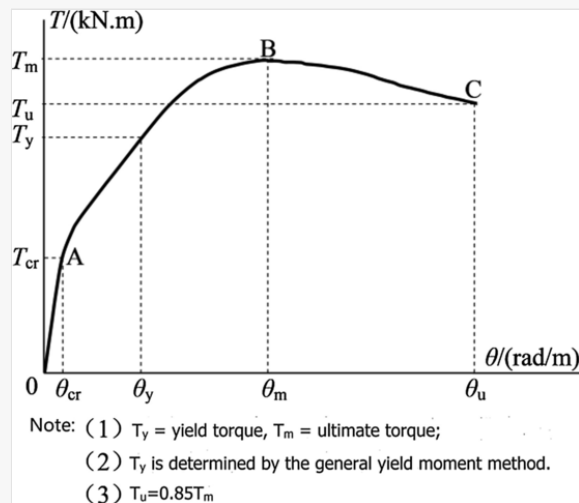
Fig. 9



Comparison of experimental and simulated torque-twist curves.

Both the test and numerical simulation results (Fig. 10) show that the entire process of an SRC member under combined torsion can be divided into three ranges: the elastic range prior to concrete crack formation (OA portion), the elastoplastic range between concrete crack formation and the ultimate torque  $T_m$  (AB portion), and the failure range following the ultimate torque  $T_m$  (BC portion). A schematic diagram of the three-staged behaviour is presented in Fig. 10.

Fig. 10




Complete behaviour of the steel-reinforced concrete structure under combined torsion.

In the model presented in Fig. 10, the ductility coefficient is defined as  $\mu = \theta_u / \theta_y$  [28,29]. Both the experimental and numerical simulation results show that the ductility coefficient of the SRC members under

combined torsion is greater than 3, indicating acceptable ductility.

**Table 3** compares the ultimate torques of the six specimens obtained from numerical simulation and experiment.

**Table 3**

 The presentation of Tables and the formatting of text in the online proof do not match the final output, though the data is the same. To preview the actual presentation, view the Proof.

Comparison of the ultimate torques obtained from the experiments and numerical simulation.

Specimen	Test result/(kN·m)	Simulation result/(kN·m)	Test result/simulation result
HSRCZ-1	44.17	45.58	0.9691
HSRCZ-2	41.52	46.68	0.8895
HSRCZ-3	48.94	50.49	0.9693
HSRCZ-4	46.49	51.90	0.8958
HSRCZ-5	56.46	53.81	1.0492
HSRCZ-6	51.31	53.28	0.9630
Mean			0.9560
Coefficient of variation			0.0586

In general, the ultimate torque from the numerical simulation is slightly higher than that of the experimental test results (except for specimen HSRCZ-5), mainly because the slip between reinforcement, structural steel, and concrete was not considered in the numerical simulation. The mean ratio of the ultimate torque of the test results to that of the numerical simulation results is 0.9560 with a coefficient of variation of 0.0586.

**Figs. 8–9** and **Table 3** indicate that the numerical simulation results and experimental test results match well, showing the validity of the numerical simulation method established in this study.

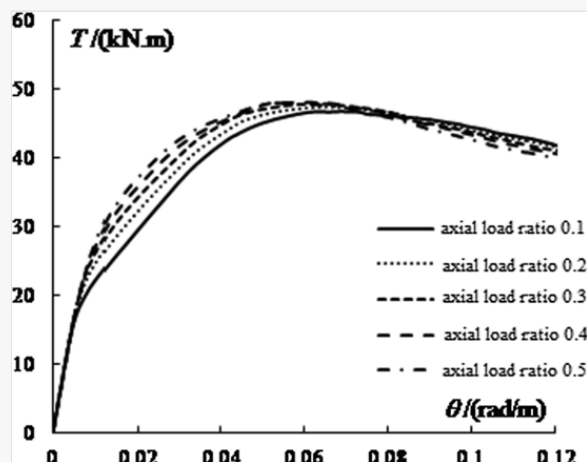
## 5 Numerical simulation analysis of column performance under combined torsion

To comprehensively understand the performance of SRC columns under combined torsion, a total of seven design parameters were considered in the numerical simulation: the axial load ratio, torsion-bending ratio, concrete strength, steel ratio, longitudinal reinforcement ratio, stirrup ratio, and shear-span ratio. Each design parameter was set to five different values, resulting in a total of 35 numerically simulated specimens to be analysed

## 5.1 Influence of the axial load ratio

The axial load ratio is set to five different values: 0.1, 0.2, 0.3, 0.4, and 0.5. The influence of the axial load ratio on the performance under torsion, as studied via numerical simulation, is shown in Fig. 11 and Table 4. It can be seen that, in the elastic range, the axial load ratio has almost no influence on the initial torsional stiffness of the SRC column. In the elastoplastic range, an increase in the axial load ratio reduces the stiffness degradation and improves the ultimate torque, mainly because the axial load suppresses the development of cracks in the column. However, after the axial load ratio exceeds 0.4, the ultimate torque starts to decrease. In the failure range, a higher axial load ratio results in a higher rate of load-carrying capacity degradation and lower ductility, mainly because a higher axial load corresponds to a more significant second-order effect on the column. Table 4 shows that the ultimate torque reaches a minimum of 46.81 kN·m when the axial load ratio is 0.1. Subsequently, the ultimate torque gradually increases with increasing axial load ratio and reaches a maximum of 48.14 kN·m when the axial load ratio is 0.4. The ductility coefficient reaches a maximum value of 4.3 when the axial load ratio is 0.1. Subsequently, the ductility coefficient gradually decreases with increasing axial load ratio and reaches a minimum value of 3.25 when the axial load ratio is 0.5.

Fig. 11



Influence of the axial load ratio on the performance of a steel-reinforced concrete column under combined torsion.

Table 4

*i* The presentation of Tables and the formatting of text in the online proof do not match the final output, though the data is the same. To preview the actual presentation, view the Proof.

Influence of the axial load ratio on the ultimate torque and ductility coefficient.

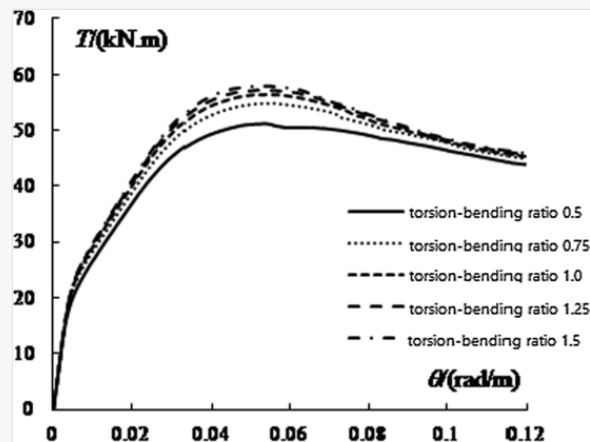
Specimen no.	Axial load ratio	Ultimate torque $T_m$ /(kN·m)	Ductility coefficient $\mu$
ZYB-1	0.1	46.81	4.30

ZYB-2	0.2	47.47	3.78
ZYB-3	0.3	47.94	3.50
ZYB-4	0.4	48.14	3.39
ZYB-5	0.5	47.91	3.25

## 5.2 Influence of the torsion-bending ratio

The torsion-bending ratio is set to five different values: 0.5, 0.75, 1.0, 1.25, and 1.5. The influence of the torsion-bending ratio variation on the performance under torsion, as studied via numerical simulation, is shown in Fig. 12 and Table 5. In the elastic range, the torsion-bending ratio has virtually no impact on the initial torsional stiffness of the SRC column. In the elastoplastic range, an increase in the torsion-bending ratio slows the stiffness degradation and improves the ultimate torque. In the failure range, a higher torsion-bending ratio results in faster load-carrying capacity degradation and lower ductility. Table 5 shows that the ultimate torque reaches a minimum of 51.18 kN·m when the torsion-bending ratio is 0.5. Subsequently, the ultimate torque increases gradually with increasing torsion-bending ratio and reaches a maximum of 57.90 kN·m when the torsion-bending ratio is 1.5. The ductility coefficient reaches a maximum of 4.18 when the torsion-bending ratio is 0.5. Subsequently, the ductility coefficient gradually decreases with increasing torsion-bending ratio and reaches a minimum value of 3.19 when the torsion-bending ratio is 1.5.

Fig. 12



Influence of the torsion-bending ratio on the performance of a steel-reinforced concrete column under combined torsion.

Table 5

*i* The presentation of Tables and the formatting of text in the online proof do not match the final output, though the data is the same. To preview the actual presentation, view the Proof.

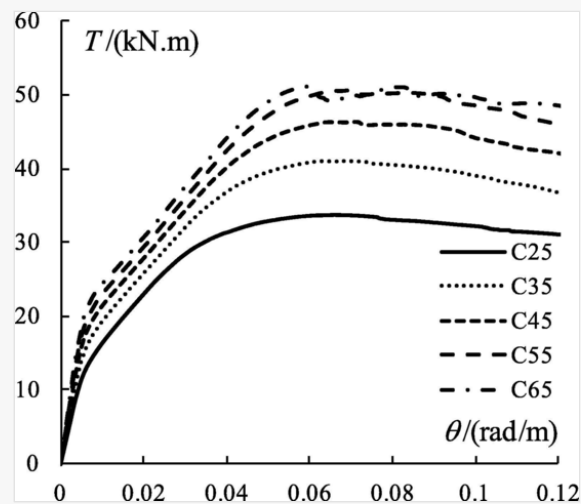
Influence of the torsion-bending ratio on the ultimate torque and ductility coefficient.

Specimen no.	Torsion-bending ratio	Ultimate torque $T_m$ /(kN·m)	Ductility coefficient $\mu$
NWB-1	0.5	51.18	4.18
NWB-2	0.75	54.86	3.52
NWB-3	1.0	56.41	3.40
NWB-4	1.25	57.17	3.25
NWB-5	1.5	57.90	3.19

### 5.3 Influence of the concrete strength

The concrete strength is set to five different values: C25, C35, C45, C55, and C65. The influence of the concrete strength on the performance under torsion, as studied via numerical simulation, is shown in Fig. 13 and Table 6. In the elastic range, the concrete strength significantly influences the initial torsional stiffness of the SRC column; a higher concrete strength results in a higher initial stiffness. In the elastoplastic range, an increase in the concrete strength reduces the stiffness degradation and improves the ultimate torque. In the failure range, the concrete strength has a limited impact on the rate of the load-carrying capacity degradation. Table 6 shows that the ultimate torque attains a minimum of 33.57 kN·m when the concrete strength is C25. Subsequently, the ultimate torque gradually increases with increasing concrete strength and reaches a maximum of 51.11 kN·m when the concrete strength is C65. The ductility coefficient reaches a maximum of 5.03 when the concrete strength is C25. Subsequently, the ductility coefficient gradually decreases with increasing concrete strength and reaches a minimum of 3.26 when the concrete strength is C65.


Fig. 13



Influence of concrete strength on the performance of a steel-reinforced concrete column under combined torsion.



Table 6

 The presentation of Tables and the formatting of text in the online proof do not match the final output, though the data is the same. To preview the actual presentation, view the Proof.

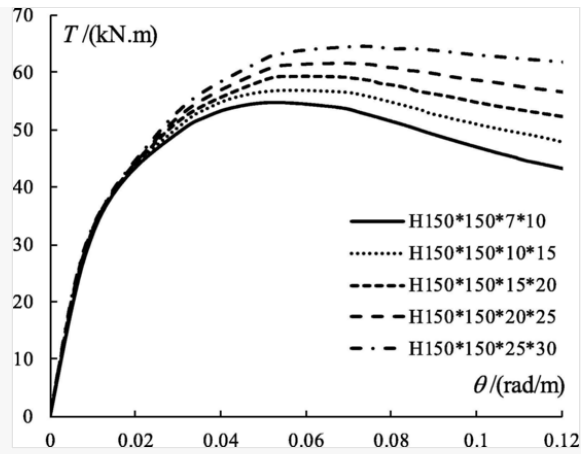
Influence of concrete strength on the ultimate torque and ductility coefficient.

Specimen no.	Concrete strength	Ultimate torque $T_m$ /(kN·m)	Ductility coefficient $\mu$
HQD-1	C25	33.57	5.03
HQD-2	C35	40.94	4.28
HQD-3	C45	46.32	4.04
HQD-4	C55	50.21	3.73
HQD-5	C65	51.11	3.26

#### 5.4 Influence of the steel ratio

For the structural steel in the column, we adopt steel sections of  $H150 \times 150 \times 7 \times 10$ ,  $H150 \times 150 \times 10 \times 15$ ,  $H150 \times 150 \times 15 \times 20$ ,  $H150 \times 150 \times 20 \times 25$ , and  $H150 \times 150 \times 25 \times 30$ ; the corresponding steel ratios are 4.34%, 6.33%, 8.50%, 10.56%, and 12.50%. The influence of the steel ratio on the performance under torsion, as studied via numerical simulation, is shown in Fig. 14 and Table 7. In the elastic range, the steel ratio has essentially no influence on the initial torsional stiffness of the SRC column. In the elastoplastic range, an increase in the steel ratio reduces the stiffness degradation rate and improves the ultimate torque. In the failure range, a higher steel ratio results in slower degradation of the bearing capacity and better ductility. Table 7 shows that the ultimate torque reaches a minimum of 54.76 kN·m when the steel ratio is 4.34%. Subsequently, the ultimate torque gradually increases with increasing steel ratio and reaches a maximum of 64.56 kN·m when the steel ratio is 12.50%. The ductility factor reaches a maximum of 8.71 when the steel ratio is 12.50%. Subsequently, the ductility coefficient gradually decreases with increasing steel ratio and reaches a minimum value of 4.29 when the steel ratio is 4.34%.

Fig. 14



Influence of the steel ratio on the performance of a steel-reinforced concrete column under combined torsion.

Table 7

*i* The presentation of Tables and the formatting of text in the online proof do not match the final output, though the data is the same. To preview the actual presentation, view the Proof.

Influence of the steel ratio on the ultimate torque and ductility coefficient.

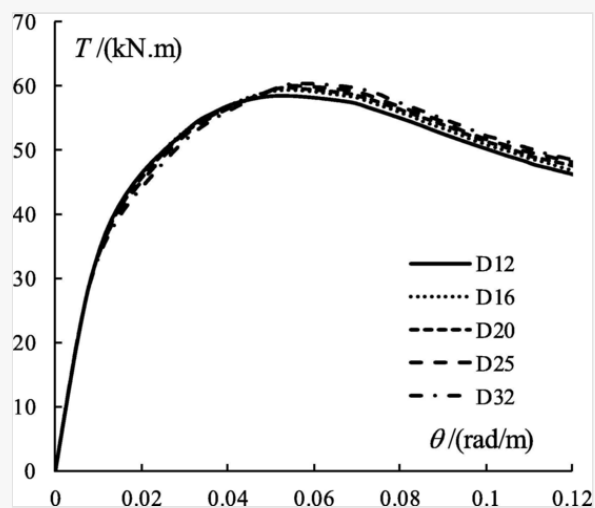
Specimen no.	Steel ratio/%	Ultimate torque $T_m$ /(kN·m)	Ductility coefficient $\mu$
PGL-1	4.34	54.76	4.29
PGL-2	6.33	56.83	4.67
PGL-3	8.50	59.28	5.21
PGL-4	10.56	61.60	7.34
PGL-5	12.50	64.56	8.71

## 5.5 Influence of the longitudinal reinforcement ratio

The longitudinal reinforcement in the column cross section is set to five different cases:  $8\Phi 12$ ,  $8\Phi 16$ ,  $8\Phi 20$ ,  $8\Phi 25$ , and  $8\Phi 32$ ; the corresponding longitudinal reinforcement ratios are 1.00%, 1.79%, 2.79%, 4.36%, and 7.15%. The influence of the longitudinal reinforcement ratio on the performance under torsion, as studied via numerical simulation, is shown in Fig. 15 and Table 8. In the elastic range, the longitudinal reinforcement ratio has virtually no effect on the initial torsional stiffness of the SRC column. In the elastoplastic range, an increase in the longitudinal reinforcement ratio alone improves the ultimate torque only slightly. In the failure range, an increase in the longitudinal reinforcement ratio alone improves the ductility only slightly. Table 8 shows that the ultimate torque reaches a minimum of 58.41 kN·m when the longitudinal reinforcement ratio is 1.00% and reaches a maximum of 60.29 kN·m when the longitudinal reinforcement ratio is 7.15%. The

ductility factor reaches a maximum of 4.18 when the longitudinal reinforcement ratio is 7.15% and reaches a minimum of 4.10 when the longitudinal reinforcement ratio is 1.00%. Both Fig. 15 and Table 8 show that an increase in the longitudinal reinforcement ratio alone has a minimal effect on improving the ultimate torque and ductility.

Fig. 15



Influence of the longitudinal reinforcement ratio on the performance of a steel-reinforced concrete column under combined torsion.

Table 8

*i* The presentation of Tables and the formatting of text in the online proof do not match the final output, though the data is the same. To preview the actual presentation, view the Proof.

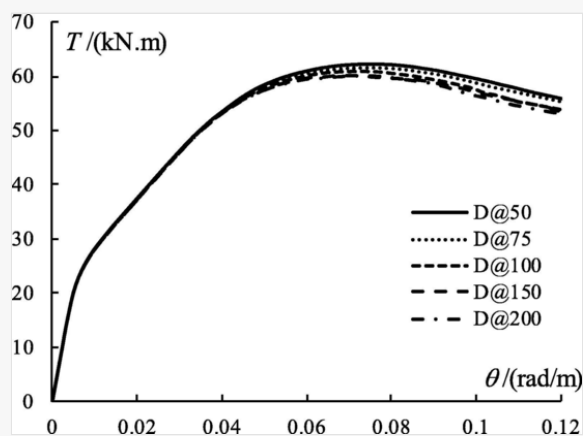
Influence of the longitudinal reinforcement ratio on the ultimate torque and ductility coefficient.

Specimen no.	Longitudinal reinforcement ratio/%	Ultimate torque $T_m$ /(kN·m)	Ductility coefficient $\mu$
ZJPJL-1	1.00	58.41	4.10
ZJPJL-2	1.79	59.05	4.11
ZJPJL-3	2.79	59.47	4.14
ZJPJL-4	4.36	59.87	4.16
ZJPJL-5	7.15	60.29	4.18

## 5.6 Influence of the stirrup ratio

The stirrup in the column cross section is set to five different cases :  $\Phi 8@200$ ,  $\Phi 8@150$ ,  $\Phi 8@100$ ,  $\Phi 8@75$ , and  $\Phi 8@50$ ; the corresponding stirrup ratios are 0.17%, 0.22%, 0.34%, 0.45%, and 0.67%. The influence of the stirrup ratio on the performance under torsion, as studied via numerical simulation, is shown in Fig. 16 and Table 9. In the elastic range, the stirrup ratio has virtually no impact on the initial torsional stiffness of the SRC column. In the elastoplastic range, an increase in the stirrup ratio only slightly improves the ultimate torque. In the failure range, an increase in the stirrup ratio moderately improves the ductility. Table 9 shows that the ultimate torque reaches a minimum of 60.04 kN·m when the stirrup ratio is 0.17% and reaches a maximum of 62.20 kN·m when the stirrup ratio is 0.67%. Additionally, the ductility factor reaches a maximum of 4.76 when the stirrup ratio is 0.67% and reaches a minimum of 3.75 when the stirrup ratio is 0.17%. Both Fig. 16 and Table 9 show that an increase in the stirrup ratio alone has a minimal effect on improving the ultimate torque and ductility.

Fig. 16



Influence of the stirrup ratio on the performance of a steel-reinforced concrete column under combined torsion.

Table 9

*i* The presentation of Tables and the formatting of text in the online proof do not match the final output, though the data is the same. To preview the actual presentation, view the Proof.

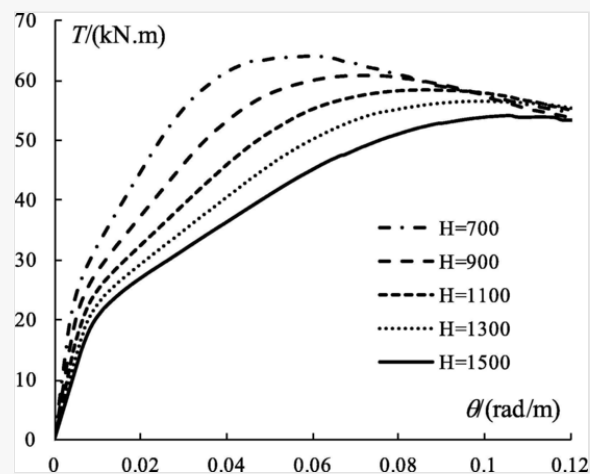
Influence of the stirrup ratio on the ultimate torque and ductility coefficient.

Specimen no.	Stirrup ratio/%	Ultimate torque $T_m$ /(kN·m)	Ductility coefficient $\mu$
GJPGL-1	0.17	60.04	3.75
GJPGL-2	0.22	60.12	4.03
GJPGL-3	0.34	60.87	4.12
GJPGL-4	0.45	61.53	4.34

## 5.7 Influence of the shear-span ratio

The column height  $H$  is changed to investigate the influence of the shear-span ratio ( $\lambda = M/Vh = H/h$ ) on the performance of the SRC column under combined torsion. The column height  $H$  is set to five different values: 700 mm, 900 mm, 1100 mm, 1300 mm, and 1500 mm; the corresponding shear-span ratios are 2.33, 3.00, 3.67, 4.33, and 5.00. The influence of the shear-span ratio on the performance under torsion, as studied via numerical simulation, is shown in Fig. 17 and Table 10. In the elastic range, the shear-span ratio significantly influences the initial torsional stiffness of the SRC column; a smaller shear-span ratio results in a higher initial torsional stiffness. In the elastoplastic range, a decrease in the shear-span ratio reduces the stiffness degradation rate and improves the ultimate torque. In the failure range, a smaller shear-span ratio results in a higher rate of bearing capacity degradation and worse ductility. Table 10 shows that the ultimate torque reaches a minimum of 54.01 kN·m when the shear-span ratio is 5.00 and reaches a maximum of 64.12 kN·m when the shear-span ratio is 2.33. The ductility coefficient reaches a maximum of 6.20 when the shear-span ratio is 5.00 and reaches a minimum of 4.09 when the shear-span ratio is 2.33. Both Fig. 17 and Table 10 show that the shear-span ratio significantly influences the ultimate torque and ductility.

Fig. 17



Influence of the shear-span ratio on the performance of a steel-reinforced concrete column under combined torsion.

Table 10

*i* The presentation of Tables and the formatting of text in the online proof do not match the final output, though the data is the same. To preview the actual presentation, view the Proof.


Influence of the shear-span ratio on the ultimate torque and ductility coefficient.

Specimen no.	Shear-span ratio/%	Ultimate torque $T_m$ /(kN·m)	Ductility coefficient $\mu$
JKB-1	2.33	64.12	4.09
JKB-2	3.00	60.87	4.42
JKB-3	3.67	58.40	5.15
JKB-4	4.33	56.57	5.57
JKB-5	5.00	54.01	6.20

## 5.8 Analysis of the influences of the design parameters on the torsional performance of steel-reinforced concrete columns

The analysis in Sections 4.5.1 to 4.7.7 reveals that the concrete strength and shear-span ratio significantly influence the initial torsional stiffness of the structural member. An increase in the concrete strength is beneficial, while an increase in the shear-span ratio is unfavourable. The other five design parameters have essentially no impact on the initial torsional stiffness of the structural member. The influences of the seven design parameters within their respective ranges on the ultimate torque and ductility coefficient are ranked (1 = most influential, 7 = least influential) in Table 11.

Table 11

 The presentation of Tables and the formatting of text in the online proof do not match the final output, though the data is the same. To preview the actual presentation, view the Proof.

Ranked influences of the design parameters on the ultimate torque and ductility coefficient.

Design parameter	Range	Influence on the ultimate torque		Influence on the ductility	
		$\Delta T_m$ /(kN·m)	Rank	$\Delta \mu$	Rank
Axial load ratio	0.1, 0.2, 0.3, 0.4, 0.5	1.33/−0.23	7	−1.05	4
Torsion-bending ratio	0.5, 0.75, 1.0, 1.25, 1.5	6.72	4	−0.99	6
Concrete strength	C25, C35, C45, C55, C65	17.54	1	−1.77	3
Steel ratio/%	4.34, 6.33, 8.50, 10.56, 12.50	9.80	3	4.42	1
Longitudinal reinforcement ratio/%	1.00, 1.79, 2.79, 4.36, 7.15	1.88	6	0.08	7
Stirrup ratio/%	0.17, 0.22, 0.34, 0.45, 0.67	2.16	5	1.01	5
Shear-span ratio	2.33, 3.00, 3.67, 4.33, 5.00	−10.11	2	2.11	2

Note: (1)  $\Delta T_m$  is the change in the ultimate torque as a design parameter changes in ascending order within its corresponding range of values. A negative sign “-” in front of the  $\Delta T_m$  value indicates a decrease (which is unfavourable) in the ultimate torque with an increase in the design parameter. A  $\Delta T_m$  value without a sign in front indicates an increase (which is favourable) in the ultimate torque with an increase in the design parameter. For example, “1.33/-0.23” means that when the axial load ratio increases from 0.1 to 0.4, the ultimate torque increases by 1.33 kN-m, and when the axial load ratio increases from 0.4 to 0.5, the ultimate torque decreases by 0.23 kN-m.

(2)  $\Delta\mu$  is the change in the ductility coefficient as a design parameter changes in ascending order within its corresponding range of values. A negative sign “-” in front of the  $\Delta\mu$  value indicates a decrease (which is unfavourable) in the ductility coefficient with an increase in the design parameter. A  $\Delta\mu$  value without a sign in front indicates an increase (which is favourable) in the ductility coefficient with an increase in the design parameter.

(3) The ranking of influences is based on  $|\Delta T_m|$  and  $|\Delta\mu|$ , the absolute values of  $\Delta T_m$  and  $\Delta\mu$ , respectively. The maximum change in the absolute value is ranked number ‘1’, and the minimum change is ranked number ‘7’. A lower rank corresponds to a stronger influence on the torsion performance.

As listed in [Table 11](#), the concrete strength has the most significant influence on the ultimate torque, while the axial load ratio has the least significant influence on the ultimate torque. The seven design parameters studied, ranked from highest to lowest in terms of influence on the ultimate torque, are the concrete strength, shear-span ratio, steel ratio, torsion-bending ratio, stirrup ratio, longitudinal reinforcement ratio, and axial load ratio. Increases in the concrete strength, steel ratio, torsion-bending ratio, stirrup ratio, and longitudinal reinforcement ratio are favourable, while an increase in the shear-span ratio is unfavourable. When the axial load ratio is lower than 0.4, an increase in the axial load ratio is favourable; when the axial load ratio is higher than 0.4, an increase in the axial load ratio is unfavourable.

As shown in [Table 11](#), the steel ratio has the most significant impact on the ductility coefficient, while the longitudinal reinforcement ratio has the least significant impact. The seven design parameters studied, ranked from highest to lowest in terms of influence on the ductility coefficient, are the steel ratio, shear-span ratio, concrete strength, axial load ratio, stirrup ratio, torsion-bending ratio, and longitudinal reinforcement ratio. Increases in the steel ratio, shear-span ratio, stirrup ratio, and longitudinal reinforcement ratio are favourable, while increases in the concrete strength, axial load ratio, and torsion-bending ratio are unfavourable.

## 6 Conclusions

The performance of SRC columns under combined torsion was analysed via experimental study and numerical simulation. The following conclusions can be drawn:

- (1) The behaviour of an SRC column under combined torsion can be divided into three stages: the elastic range, the elastoplastic range, and the failure stage.
- (2) It is feasible to perform an ABAQUS-based nonlinear analysis of the performance of SRC columns under combined torsion using the SMM to consider the concrete material softening effect and the KSPM to consider the stirrup confining effect.
- (3) When the seven design parameters studied vary within their respective ranges of values in ascending order, their influence on the initial torsional stiffness, ultimate torque, and ductility coefficient is as follows.
  - The concrete strength and shear-span ratio significantly influence the initial torsional stiffness

of the structural member. An increase in the concrete strength is favourable, while an increase in the shear-span ratio is unfavourable. The other five design parameters have a very small impact on the initial torsional stiffness of the structural member.

- The seven design parameters studied, ranked from highest to lowest in terms of influence on the ultimate torque, are the concrete strength, shear-span ratio, steel ratio, torsion-bending ratio, stirrup ratio, longitudinal reinforcement ratio, and axial load ratio. Increases in the concrete strength, steel ratio, torsion-bending ratio, stirrup ratio, and longitudinal reinforcement ratio are favourable, while an increase in the shear-span ratio is unfavourable. When the axial load ratio is lower than 0.4, an increase in the axial load ratio is favourable; when the axial load ratio is higher than 0.4, an increase in the axial load ratio is unfavourable.
- The seven design parameters studied, ranked from highest to lowest in terms of influence on the ductility coefficient, are the steel ratio, shear-span ratio, concrete strength, axial load ratio, stirrup ratio, torsion-bending ratio, and longitudinal reinforcement ratio. Increases in the steel ratio, shear-span ratio, stirrup ratio, and longitudinal reinforcement ratio are favourable, while increases in the concrete strength, axial load ratio, and torsion-bending ratio are unfavourable.


## Acknowledgements

This research was conducted at Suzhou University of Science and Technology, [China](#) and was financially supported by the [Jiangsu Province Enterprise Practice and Training Project for Young Teachers of Suzhou, China](#) (2017QYSJPX006) and the National Natural Science Foundation of China Project (51078249).

## Appendix A Supplementary material

Supplementary data to this article can be found online at <https://doi.org/10.1016/j.engstruct.2019.109980>.

## References

 The corrections made in this section will be reviewed and approved by journal production editor.

- [1] Spacone E, El-Tawil S. Nonlinear analysis of steel-concrete composite structures: State of the art. *J Struct Eng* 2004;130(2):159–168.
- [2] Nakashima M, Roeder CW, Maruoka Y. Steel moment frames for earthquakes in United States and Japan. *J Struct Eng* 2000;126(8):861–868.
- [3] Nie J-G, Wang Y-H, Fan J-S. Experimental study on seismic behavior of concrete filled steel tube columns under pure torsion and compression–torsion cyclic load. *J Constr Steel Res* 2012;79:115–126.
- [4]



Wei L, Wang S. Aseismic analysis on torsion angle effect of vertical members intorsionally irregular structure. *Build Struct* 2006;36(7):8–20. [in Chinese].

- [5] Hu S. Torsion analysis and design of composite beams. Beijing: People Communications Press; 2005. p. 15–17. [in Chinese].
- [6] Technical specification for steel reinforced concrete composite structures: JGJ138-2001. Beijing: China Architecture&Building Press; 2001 [in Chinese].
- [7] Vecchio FJ. Nonlinear finite element analysis of reinforced concrete membranes. *ACI Struct J* 1989;86:26–35.
- [8] Gourley BC, et al. A synopsis of studies of the monotonic and cyclic behavior of concrete-filled steel tube members, connections, and frames. Newmark Structural Engineering Laboratory. University of Illinois at Urbana; 2008.
- [9] Lei Q. Nonlinear finite element analysis of steel reinforced concrete members subjected to torsion. Xi'an: Xi'an University of Architecture and Technology; 2007. p. 38–42. [in Chinese].
- [10] Vecchio FJ. Nonlinear finite element analysis of reinforced concrete membranes. *ACI Struct J* 1989;86(1):26–35.
- [11] Chalioris CE. Torsional strengthening of rectangular and flanged beams using carbon fibre-reinforced-polymers—Experimental study. *Constr Build Mater* 2008;22(1):21–29.
- [12] Mondal TG, Prakash SS. Effect of tension stiffening on the behaviour of reinforced concrete circular columns under torsion. *Eng Struct* 2015;92:186–195.
- [13] Chalioris CE. Experimental study of the torsion of reinforced concrete members. *Struct Eng Mech* 2006;23(6):713–737.
- [14] Panchacharam S, Belarbi A. Torsional behavior of reinforced concrete beams strengthened with FRP composites. First FIB Congress, Osaka, Japan; 2002.
- [15] Ling HSNJL. Study on the torisonal behaviors of steel-concrete composite beams. *Build Struct* 1999;4.
- [16] Han L-H, Tao Z, Liu W. Concrete filled steel tubular structures from theory to practice. *J Fuzhou Univ (Nat Sci Ed)* 2001;6:3.
- [17] Subramanian N. Design of reinforced concrete structures. Oxford University Press; 2013.
- [18] Shao Y, Wang N, Chen Z, Liu F. Torsional behaviour and strength calculation methods of angle steel reinforced concrete beams. *Eng Mech* 2013;30(9):103–110. [in Chinese].
- [19] Shao Y, Yu W, Chen Z, et al. Experimental study on torsional behavior of solid web steel reinforced concrete beams. *Build Struct* 2013;43(8):58–62. [in Chinese].

- [20] Kim K, Chai HY. Ultimate strengths of steel rectangular box beams subjected to combined action of bending and torsion. Eng Struct 2008;30(6):1677–1687.
- [21] Deifalla A, Ghobarah A. Behavior and analysis of inverted T-shaped RC beams under shear and torsion. Eng Struct 2014;68(4):57–70.
- [22] Yong Y, Zixiong G, Jianguo N. Study on numerical simulation technology of steel reinforced concrete structures using ANSYS. Eng Mech 2006;23(4):79–85.
- [23] Jeng C-H, Hsu TT. A softened membrane model for torsion in reinforced concrete members. Eng Struct 2009;31(9):1944–1954.
- [24] Mansour M, Hsu TT. Behavior of reinforced concrete elements under cyclic shear. II: Theoretical model. J Struct Eng 2005;131(1):54–65.
- [25] Elgamal A, et al. Three-dimensional seismic response of Humboldt Bay bridge-foundation-ground system. J Struct Eng 2008;134(7):1165–1176.
- [26] Stramandinoli RSB, Rovere HLL. An efficient tension-stiffening model for nonlinear analysis of reinforced concrete members. Eng Struct 2008;30(7):2069–2080.
- [27] Mang HA, et al. Wind-loaded reinforced-concrete cooling towers: buckling or ultimate load?. Eng Struct 1983;5(3):163–180.
- [28] McClintock FA. A criterion for ductile fracture by the growth of holes. J Appl Mech 1968;35(2):363–371.
- [29] Ong J. An improved technique for the prediction of axial fatigue life from tensile data. Int J Fatigue 1993;15(3):213–219.

---

## Highlights

- ~~The initial torsion stiffness increases with increasing concrete strength and decreases with increasing shear-span ratio.~~ Initial torsion stiffness increases with increasing concrete strength and decreases with increasing shear-span ratio.
- ~~The torsional strength of cross-shaped steel reinforced concrete columns enhanced but no obvious difference in ductility was detected. The energy dissipation capacity had a consideration improvement in the later process of loading. The torsional strength was remarkably increased followed by an increase in torsion-bending ratio. However, the ductility was reduced at a relatively high rate as the torsion-bending ratio increased and the energy dissipation capacity had a slight decrease.~~ Ductility was reduced torsion-bending ratio increased and the energy dissipation capacity decreased.

- The influence of parameters on the ultimate torsion in descending order is as follows: concrete strength, shear-span ratio, steel ratio, torsion-bending ratio, stirrup ratio, longitudinal reinforcement ratio and axial load ratio. Influence order of parameters on the ultimate torsion is: concrete strength, shear/span, steel ratio, torsion/bending, stirrup ratio, longitudinal reinforcement ratio and axial load ratio.
  - The influence of these parameters on the ductility coefficient in descending order are as follows: the steel ratio, shear-span ratio, concrete strength, axial load ratio, stirrup ratio, torsion-bending ratio and longitudinal reinforcement ratio. Influence order of parameters on the ductility coefficient is: steel ratio, shear/span, concrete strength, axial load ratio, stirrup ratio, torsion-bending ratio and longitudinal reinforcement ratio.
- 

## Appendix A Supplementary material

The following are the Supplementary data to this article:

[Multimedia Component 1](#)

### Supplementary Data 1

## Queries and Answers

**Query:** Your article is registered as a regular item and is being processed for inclusion in a regular issue of the journal. If this is NOT correct and your article belongs to a Special Issue/Collection please contact [j.balamurugan@elsevier.com](mailto:j.balamurugan@elsevier.com) immediately prior to returning your corrections.

**Answer:** Yes

**Query:** The author names have been tagged as given names and surnames (surnames are highlighted in teal color). Please confirm if they have been identified correctly.

**Answer:** Yes

**Query:** Please check the address for the corresponding author that has been added here, and correct if necessary.

**Answer:** Correct

**Query:** Please check the keywords, and correct if necessary.

**Answer:** Done

**Query:** Please check the edit made in the sentence “The stirrup in the column cross section is set to five different cases...”, and correct if necessary.

**Answer:** Here the should be changed to  $\Phi$ , as following:  $\Phi 8@200$ 、 $\Phi 8@150$ 、 $\Phi 8@100$ 、 $\Phi 8@75$ 、 $\Phi 8@50$

**Query:** Sections 4.1 to 4.7 is cited in the text but not provided. Kindly check.

**Answer:** Corrected.

**Query:** Have we correctly interpreted the following funding source(s) and country names you cited in your article: Suzhou University of Science and Technology, China? Jiangsu Province Enterprise Practice and Training Project for Young Teachers, China? National Natural Science Foundation of China Project, China? /

**Answer:** Yes

**Query:** Please note that as the reference [23] supplied more than once, the repetition has been removed from the list. Please check, and amend accordingly.

**Answer:** Done

**Query:** Highlights should only consist of 85 characters per bullet point, including spaces. The highlights provided are too long; please edit them to meet the requirement.

**Answer:** Done.